S1 Description of measurement datasets not previously published

S1.1 CGR

Capo Granitola observatory (GAW ID: CGR, 37.5711°N 12.6597°E; 5 m a.s.l.) is located at the southern Sicily coastline facing the Strait of Sicily, at Torretta Granitola (12 km from Mazara del Vallo, 52,000 inhabitants), within the scientific campus of the National Research Council - Institute for the study of Anthropic Impact on Marine Environment (CNR-IAS). The CGR location is strongly affected by air masses originating or passing above the central Mediterranean basin (Tyrrenian Sea), exhibiting a prevalent north-westerly circulation.

HFC monitoring started in 2024 measuring HFC-134a, HFC-143a, HFC-152a, HFC-23, HFC-227ea, HFC-236fa, HFC-245fa, HFC-365mfc, HFC-4310mee, PFC-218, and PFC-318. HFC-32 was excluded from further analysis due to a local contamination from several air conditioning systems at the location. Samples were collected at about 6 m above ground using a Synflex sampling line continuously flushed at 2 L min^{-1}. Measurements were performed every 2 hours with a gas chromatograph-mass spectrometer (GC–MS Agilent 6820 + Agilent 5975C) system in which 800 mL of air samples (both real air and calibration standard) were enriched by a commercial preconcentration system (Markes International Unity-2-AirServer-2) following the method described in Maione et al. [3]. Ambient air measurements were regularly calibrated against a whole air standard (working standard) mixture filled at Monte Cimone AGAGE station and in turn traced back on SIO scales against a reference tank obtained from Scripps Institution of Oceanography (SIO).

S1.2 BIR

The Birkenes Observatory (58.3886°N, 8.2519°E; 219 m a.s.l., above sea level) is located in southern Norway. The observatory is in the boreo-nemoral zone with mixed coniferous and deciduous trees (65% of the land use near the site). The remainder of the land use in the region is meadows (10%), low-intensity agricultural areas (10%), and freshwater lakes (15%). Close to the Skagerrak coast (∼20 km) and at low altitude, the observatory experiences a maritime climate with relatively mild winters and moderately warm summers. The nearest city is Kristiansand (population ∼65,000), which is 25 km to the south-south-west.

Air samples were collected from an inlet 75 m above ground level. Entech Silonite-XL treated stainless steel flasks were filled using a KNF86 pump with vacuum baked EPDM diaphragms. The flask sampling period was 300 s, with a pair of flasks being filled simultaneously every 2 days. The air samples were analysed on a Medusa-GCMS system at NILU (Kjeller, Norway). For all measurements, each sample was alternated with a reference gas. The reference gas, like reference gases in the AGAGE network, was calibrated relative to parent standards at SIO.

S1.3 ZSF

The Environmental Research Station "Schneefernerhaus" (GAW ID: ZSF, 47.4165°N, 10.9796°E; 2666 m a.s.l.) is located on the southern slope of Mount Zugspitze, the highest peak in the German Alps. Situated in southern Germany, it is approximately 90 km southwest of Munich (population 2.6 million), near the Austrian border, and close to the town of Garmisch-Partenkirchen (population 28,000 at an altitude of 700 m a.s.l.). The surrounding area consists of bare rocks, devoid of vegetation, and is snow-covered from October to June.

Since 2022, the ZSF station has been measuring various gases on SIO-derived scales, including HFC-143a, HFC-125, HFC-152a, HFC-134a, HFC-245fa, HFC-365mfc, PFC-116, PFC-218, and PFC-318.

Samples are collected at the mountain ridge, located at 2825 m a.s.l., using a 290-meter-long stainless steel inlet line (1.2 cm outer diameter) with a flow rate of 16 L min^{-1}.

HFCs were analysed using an analytical system comprising a custom-built preconcentration unit, a gas chromatograph (7890A from Agilent Technologies), and a mass spectrometer (5975A from Agilent Technolo-

gies). Helium was used as the carrier gas. The sample was first dried in a water trap at approximately -45°C, then passed through an adsorbent trap cooled to around -40°C. The sample loop of the adsorbent trap was filled with 200 mg of Carboxen 1000 and 150 mg of Carboxen 1016.

Ambient air measurements were calibrated using the bracketing method, against a whole air standard (working standard) mixture, calibrated on the relevant SIO scales against a reference tank from SIO at the University of Frankfurt.

S1.4 CBW

At Cabauw, an ICOS flask sampler was used to sample $1\,h$ integrated whole air samples at $1.7\,bar$ every second day. The flasks used are $3\,L$ glass flasks containing Viton O-rings and a Kel-F seal. The samples were analysed at the University of Bristol on a Medusa GC-MS system. The flasks were subsampled at a flowrate of $35\,mL\ min^{-1}$ for $40\,min$ leading to a total sampling volume of 1.4 L. Each flask measurement was bracketed by measurements of a working standard calibrated on the relevant SIO scales. The pressure during the flask subsampling was regulated with an inline pressure regulator (Parker 8310SNVS60) and the alternating standards were pressure matched at around $1\,bar$.

S1.5 TOB

Flask sampling at Taunus Observatory started in October 2013 and was continued approximately weekly until 2022 [1, 5]. Sampling was performed manually during daytime. Individual stainless steel canisters were always pressurised in pairs up to 2.5 bar after flushing with ambient air for 15 min using a metal bellows pump (Metal Bellows 29992) connected with stainless steel tubing to a rooftop inlet at approximately 8 m above ground. Data are only reported if two analyses of each of the individual canisters met the precision criteria as described in [5].

Flask samples were analysed for halogenated compounds with the GC-MS set-up described by [1] and [5]. The set-up deployed an Agilent 7890 gas chromatograph coupled with an Agilent 5975C quadrupole mass spectrometer operated in selected ion monitoring mode. Pre-concentration of sample air was done by absorption on HayeSep D at -80°C using a Stirling cooler, followed by desorption via resistive heating to approximately 200°C. The sample flow during enrichment was either $100\ mL\ min^{-1}$ or $150\ mL\ min^{-1}$ with 1 L of sample volume being preconcentrated after passing a drying tube filled with magnesium perchlorate $Mg(ClO_4)_2$. The sample volume was determined by pressure.

Gas chromatography relied on a 7.5 m pre-column and a 22.5 m main column, both GasPro PLOT columns with an inner diameter of 0.32 mm. Helium (quality 6.0 with additional purification Valco HP2) was used as the carrier gas. The GC temperature programme started at 50°C with a final temperature of 200°C.

S1.6 HUN

Flask sampling at Hegyhátsál started in January 2024. Sampling is through Synflex tubing with a metal bellows pump (Metal Bellows 29992). Sample collection was fully automated and usually started every other day at 13:00 UTC. After flushing the sampling line for 5 minutes, the sample flask was flushed for another 10 minutes and pressurised up to 3.75 bar thereafter. Sample flasks were enclosed in a sample unit comprising 14 glass cylinders with a volume of 2.67 L each [6]. Opening and closing of flasks was controlled via two multi-position valves (Valco D16MWE) connecting 16 ports with one central inlet (outlet during laboratory analysis). Usually, one single flask was pressurised at a time, although for quality checking two samples were pressurised directly after each other on some occasions.

Flask samples were analysed with the same method as at TOB.

S2 The atmospheric transport models NAME and FLEXPART: general features and PARIS-specific setup

We use two Lagrangian Particle Dispersion Models (LPDMs) to describe the atmospheric transport and diffusion of trace compounds: NAME [Numerical Atmospheric dispersion Modelling Environment 2] and FLEXPART [FLEXible PARTicle dispersion model 7]. The setup for both LPDMs was aligned as much as possible.

For each observational site 20,000 model particles were released per hour and tracked back for 30 days in the atmosphere or until they crossed the border of a domain extending from Europe across the North Atlantic and into America (98°W to 39°E, 11°N to 79°N). Source sensitivities were stored for the same domain with a spatial resolution of 0.352° by 0.234° (approximately 25 km x 25 km) and considering all model particles residing between the model surface and 40 m above ground. Next to these surface source sensitivities, the location of where particles left the output domain was converted to boundary sensitivities giving the fraction of particles leaving the domain through a certain interface with a given horizontal and vertical extend. The horizontal spacing was aligned with that of the surface sensitivities, whereas the vertical grid spacing of the boundary sensitivities was set to 500 m up to a maximum height of 20 km above ground. For FLEXPART, air parcels that remained inside the transport model domain after the end of the 30-day backward integration were assigned to the closest boundary interface. On average, this corresponded to approximately 10 % of the model particles. In NAME, these particles were ignored. Surface source and boundary sensitivities were stored in monthly files by observational site, using the same interchangeable format for output from NAME and FLEXPART.

The NAME model was driven by 3-dimensional meteorological fields from the operational weather model operated by the UK Meteorological Office (Unified Model). The horizontal and vertical resolution of these fields varies over time with the development of the meteorological model [4, Table 1 therein]. After 2010 the resolution was ∼25 km and increased over time to a resolution of ∼12 km from July 2017 onward. For sites in the UK and Ireland nested input at a resolution of ∼1 km was available from 2012 onwards. In NAME, particles were released at a height above ground according to the inlet height of the observations. This approach was adjusted for the mountain sites Jungfraujoch, Monte Cimone, and Zugspitze, where model particles were released at 500 m, 1000 m, and 600 m above model ground, respectively, according to previous sensitivity tests.

FLEXPART was driven by 3-dimensional meteorological fields from the operational high resolution analysis/forecast (HRES) of the European Centre for Medium Range Weather Forecast (ECMWF). Since 2020 these fields were available hourly with 0.1° by 0.1° horizontal resolution for the European domain and with 0.5° by 0.5° resolution elsewhere. Before 2020 3-hourly inputs at 0.2° by 0.2° (only Alpine domain) and 1° by 1° were used. These fields were extracted from ECMWF's archive using the flexextract tool [8]. In FLEXPART, particles were released at a height above model ground according to the inlet height of the observations for sites in flat terrain, whereas for elevated sites a release height at the middle between model and real topography was chosen. The latter was additionally offset by the inlet height of the observation. Sites were categorised as elevated if their real height above sea level was at least 200 m higher than the model ground elevation at the same location.

S3 Analysis of inversion model performance

Observed and simulated mole fractions were analysed and visualised using **Fluxy**, an inverse modelling intercomparison tool. Figure S1 shows an example comparison between observed and posterior simulated HFC-143a mole fractions at all measurement sites used in the RHIME–NAME inverse system for 2024.

Model performance, defined here as the quality of the fit between observed and posterior simulated mole fractions, is evaluated with the Pearson correlation coefficient, the bias (ppt), and the centred root mean square error (cRMSE; ppt); computed separately for each site and model.

Analysis is performed on mole fractions after subtraction of the baseline to isolate enhancements associated with pollution events from variability of the baseline, which represents the time-varying global background and far-field contribution entering the inverse domain. Since baselines vary more slowly over time and for many gases exhibit a long term trend, calculation of correlation coefficients of the absolute mole fractions may be misleading because these coefficients will generally be very large.

Figure S2 shows the three statistical metrics for HFC-143a for each individual model used in the study (RHIME–NAME, RHIME–FLEXPART, ELRIS–NAME, ELRIS–FLEXPART, InTEM–NAME, and InTEM–FLEXPART), computed over periods with available site observations from 2013—2024 for NAME-based inversions and 2017—2024 for FLEXPART-based inversions.

Across most sites and model systems, posterior simulated HFC-143a mole fraction enhancements show moderate to strong correlations with observations, with the highest correlations generally observed at BIR and MHD and lower correlations at CGR and CBW. Biases are generally small and near zero, although negative biases are evident at CBW, TOB and TAC for several models. Centered RMSE varies primarily by site, with larger values at CBW and TOB and smaller values at BIR, MHD, and ZEP, reflecting the intensity of pollution events at these sites. CBW, a flask station operational since 2021, is particularly sensitive to episodic pollution events, which are challenging to capture and likely explain the poorer model–data agreement.

Model performance for the other HFCs is shown in Figures S3– S12. As for HFC-143a, sites with low measurement frequency and/or sporadic pollution events generally exhibit weaker model fits, reflecting limitations in capturing isolated pollution events. HFC-134a, HFC-125, HFC-32, HFC-152a, HFC-245fa, and HFC-365mfc show Pearson correlation coefficients above 0.5 at MHD, indicating relatively good model fits. In contrast, the coefficients for HFC-23, HFC-227ea, HFC-236fa, and HFC-4310mee fall below 0.5 at MHD, reflecting modelling challenges for gases dominated by point sources.
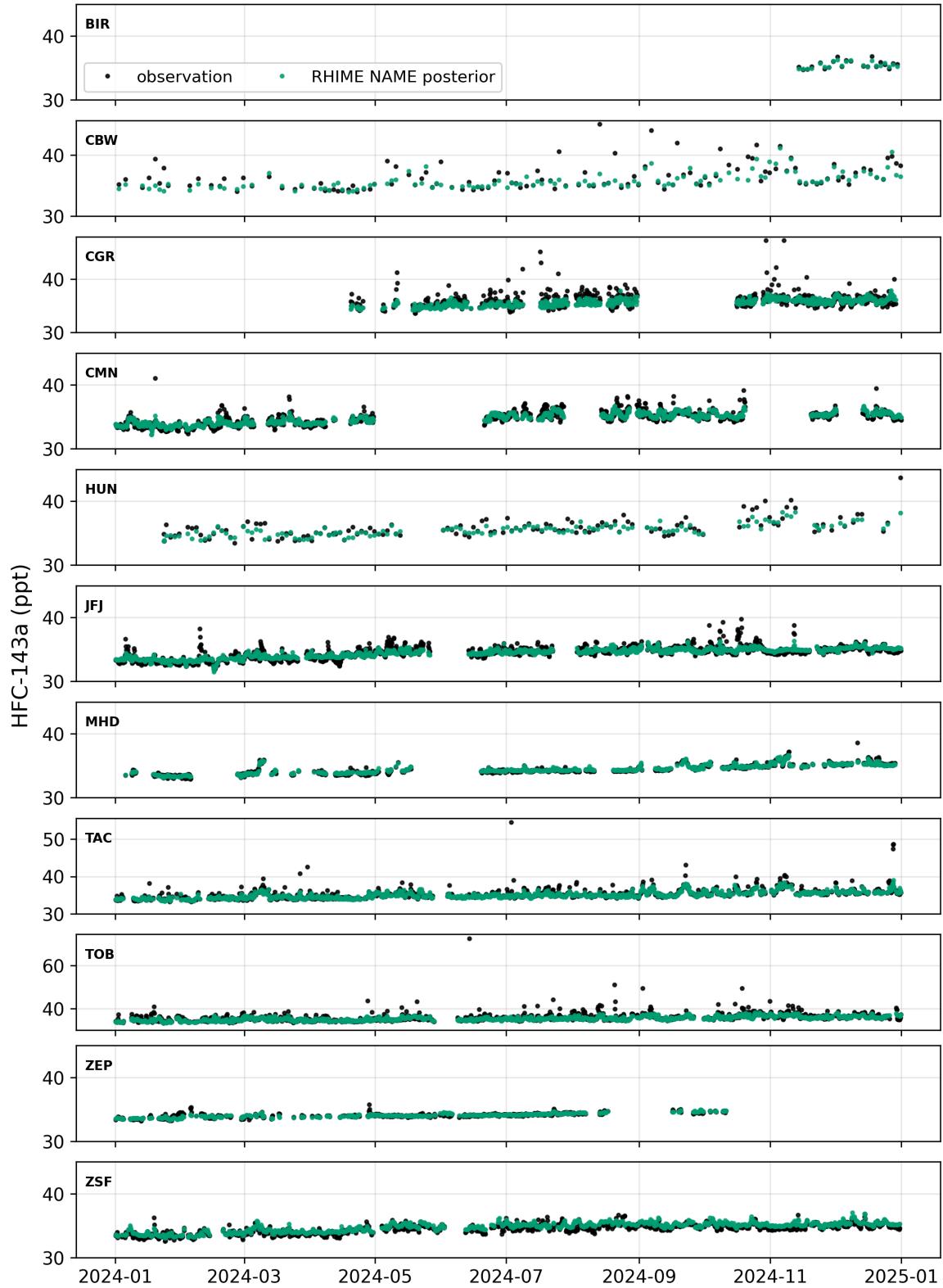
Figure S1: Observed (black) and simulated posterior (green) mole fractions of HFC-143a at eleven European measurement stations in 2024. Simulated values were taken from the RHIME inverse model using the NAME transport model.
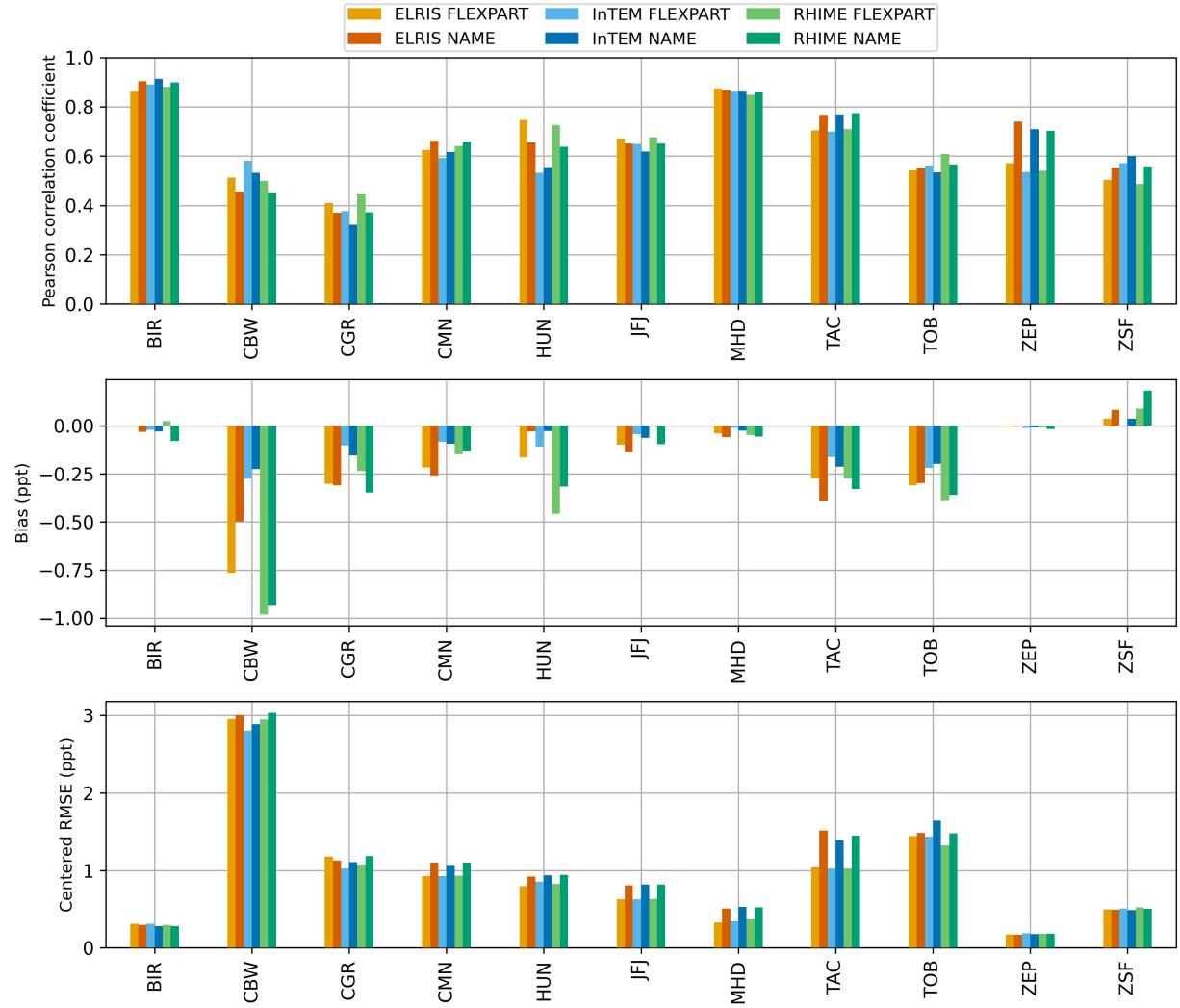
Figure S2: Pearson correlation coefficient (top), bias (middle; ppt), and centered RMSE (bottom; ppt) between posterior modelled and observed HFC-143a mole fractions above baseline at each measurement site for six inverse modelling systems (RHIME–NAME, RHIME–FLEXPART, ELRIS–NAME, ELRIS–FLEXPART, InTEM–NAME, InTEM–FLEXPART), using available site observations from 2013–2024 for NAME-based inversions and 2017–2024 for FLEXPART-based inversions.
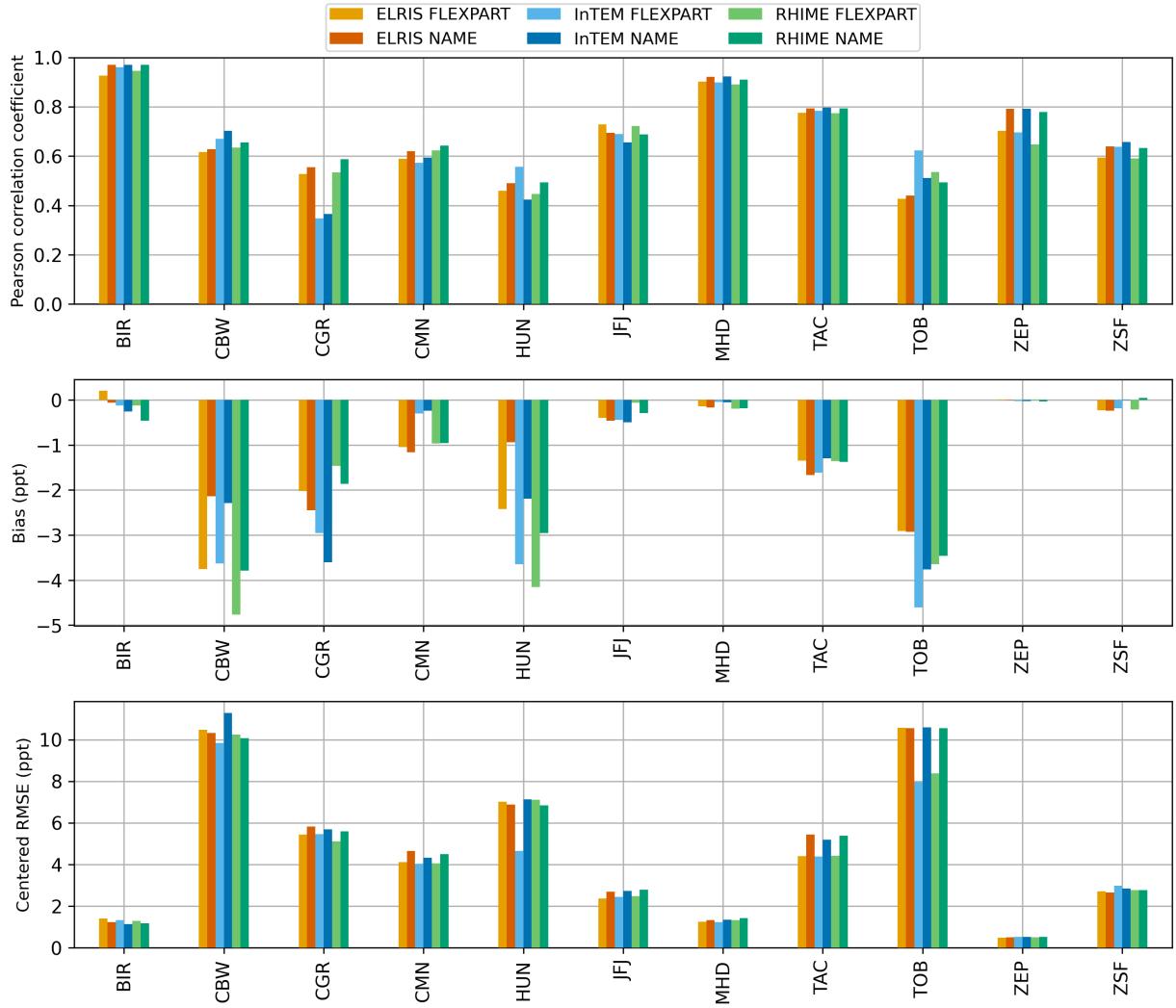
Figure S3: Pearson correlation coefficient (top), bias (middle; ppt), and centered RMSE (bottom; ppt) between posterior modelled and observed HFC-134a mole fractions above baseline at each measurement site for six inverse modelling systems (RHIME–NAME, RHIME–FLEXPART, ELRIS–NAME, ELRIS–FLEXPART, InTEM–NAME, InTEM–FLEXPART), using available site observations from 2013–2024 for NAME-based inversions and 2017–2024 for FLEXPART-based inversions.
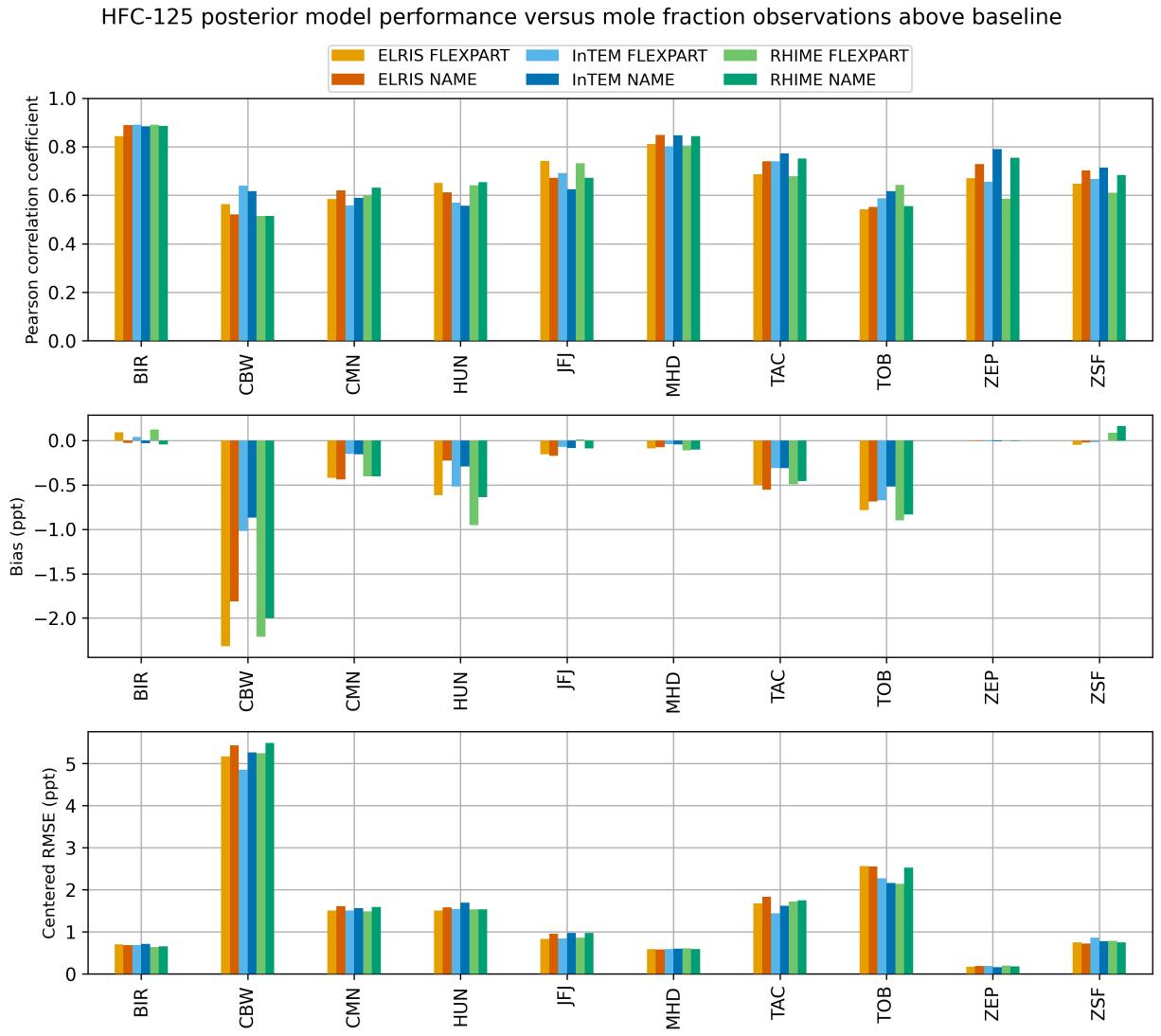
Figure S4: Pearson correlation coefficient (top), bias (middle; ppt), and centered RMSE (bottom; ppt) between posterior modelled and observed HFC-125 mole fractions above baseline at each measurement site for six inverse modelling systems (RHIME–NAME, RHIME–FLEXPART, ELRIS–NAME, ELRIS–FLEXPART, InTEM–NAME, InTEM–FLEXPART), using available site observations from 2013–2024 for NAME-based inversions and 2017–2024 for FLEXPART-based inversions.
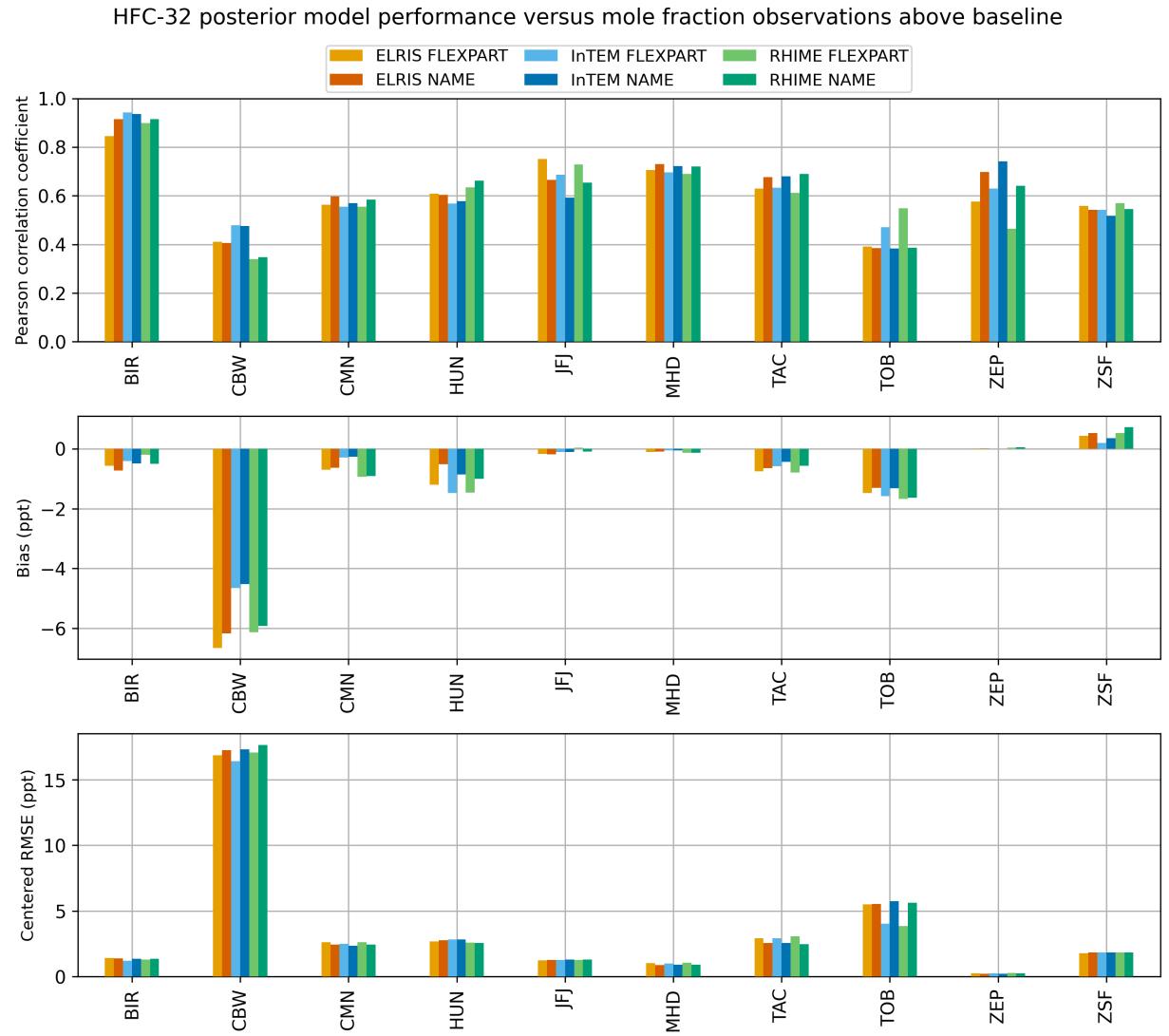
Figure S5: Pearson correlation coefficient (top), bias (middle; ppt), and centered RMSE (bottom; ppt) between posterior modelled and observed HFC-32 mole fractions above baseline at each measurement site for six inverse modelling systems (RHIME–NAME, RHIME–FLEXPART, ELRIS–NAME, ELRIS–FLEXPART, InTEM–NAME, InTEM–FLEXPART), using available site observations from 2013–2024 for NAME-based inversions and 2017–2024 for FLEXPART-based inversions.
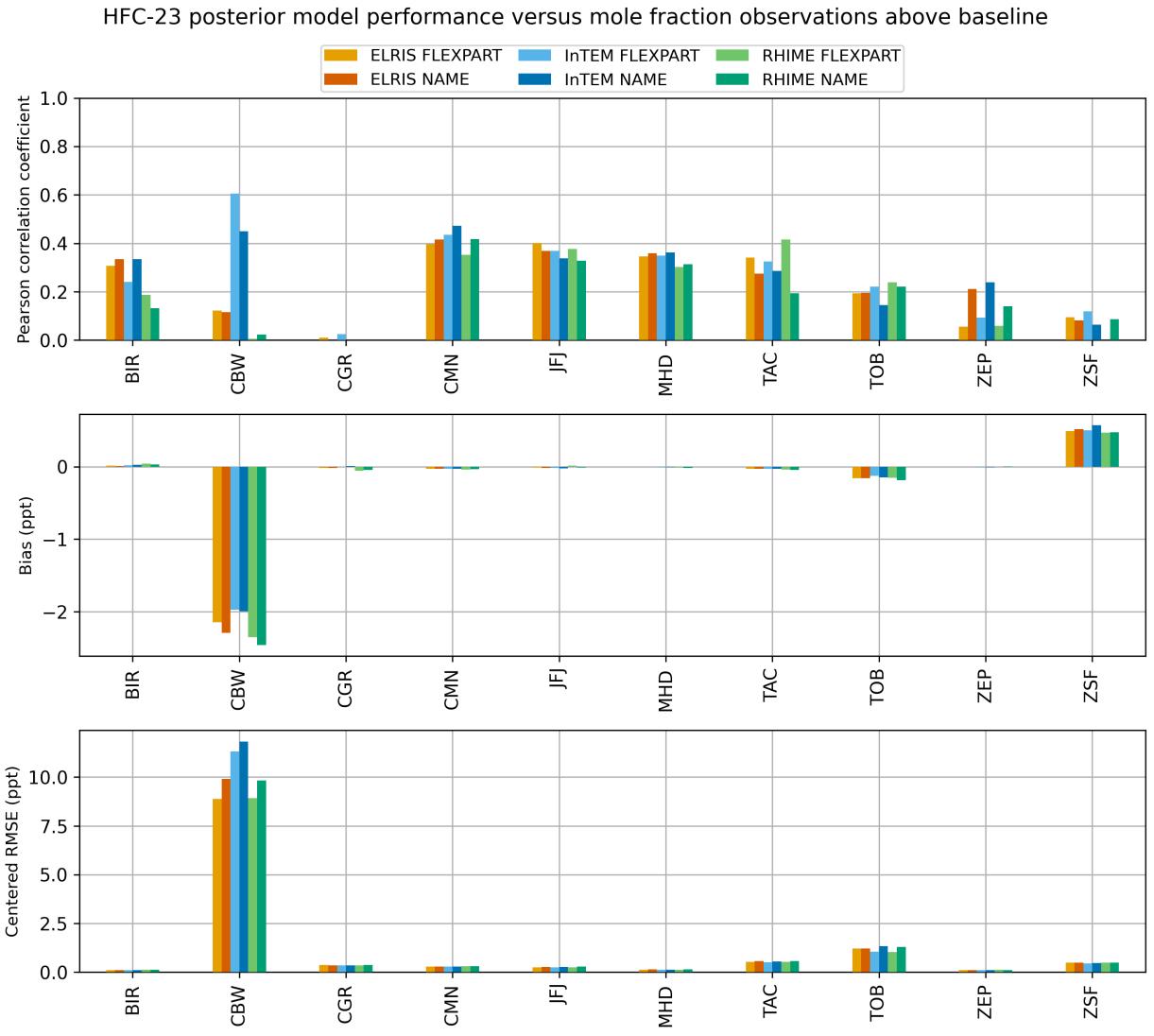
Figure S6: Pearson correlation coefficient (top), bias (middle; ppt), and centered RMSE (bottom; ppt) between posterior modelled and observed HFC-23 mole fractions above baseline at each measurement site for six inverse modelling systems (RHIME–NAME, RHIME–FLEXPART, ELRIS–NAME, ELRIS–FLEXPART, InTEM–NAME, InTEM–FLEXPART), using available site observations from 2013–2024 for NAME-based inversions and 2017–2024 for FLEXPART-based inversions.
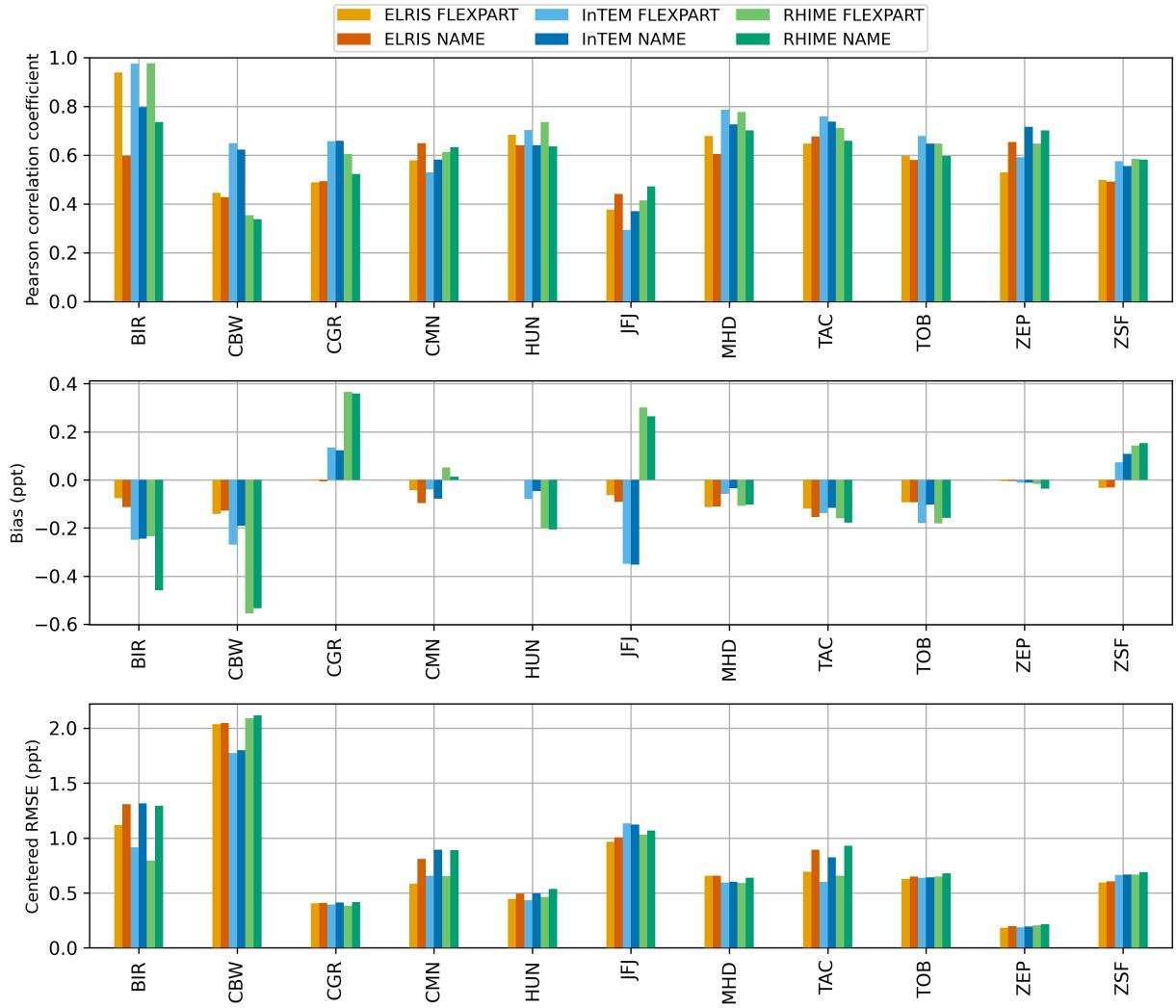
Figure S7: Pearson correlation coefficient (top), bias (middle; ppt), and centered RMSE (bottom; ppt) between posterior modelled and observed HFC-152a mole fractions above baseline at each measurement site for six inverse modelling systems (RHIME–NAME, RHIME–FLEXPART, ELRIS–NAME, ELRIS–FLEXPART, InTEM–NAME, InTEM–FLEXPART), using available site observations from 2013–2024 for NAME-based inversions and 2017–2024 for FLEXPART-based inversions.

HFC-227ea posterior model performance versus mole fraction observations above baseline
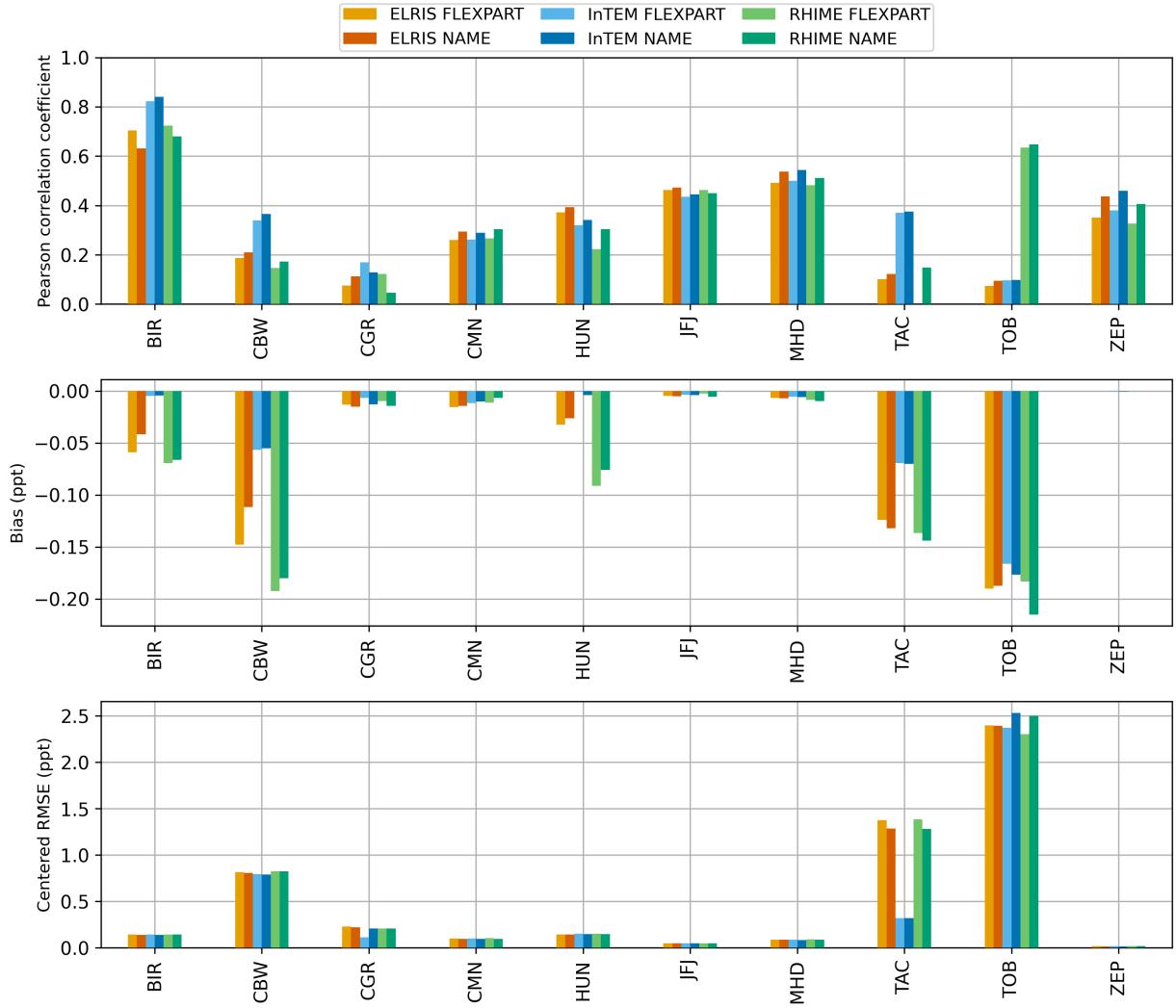
Figure S8: Pearson correlation coefficient (top), bias (middle; ppt), and centered RMSE (bottom; ppt) between posterior modelled and observed HFC-152a mole fractions above baseline at each measurement site for six inverse modelling systems (RHIME–NAME, RHIME–FLEXPART, ELRIS–NAME, ELRIS–FLEXPART, InTEM–NAME, InTEM–FLEXPART), using available site observations from 2013–2024 for NAME-based inversions and 2017–2024 for FLEXPART-based inversions.
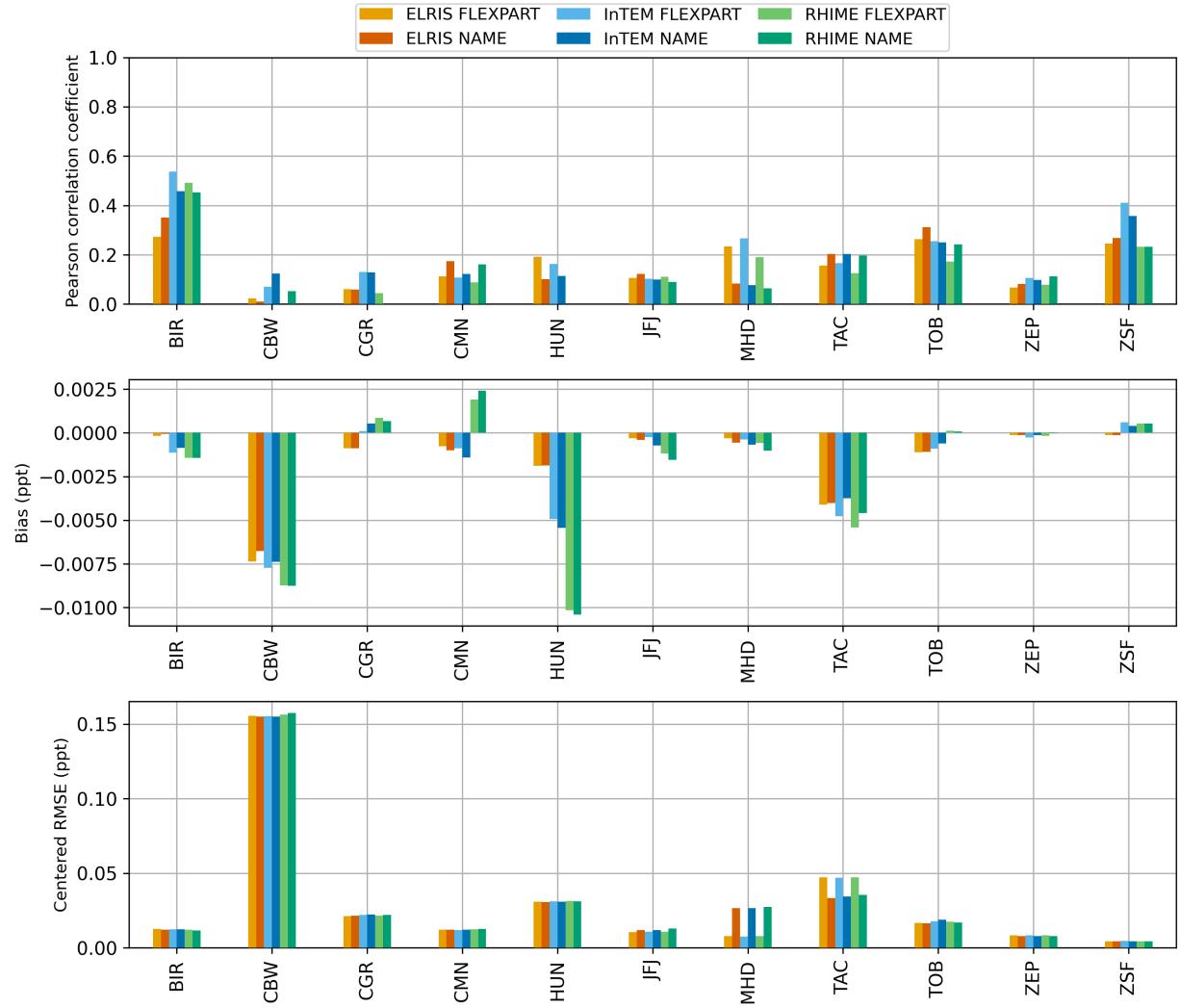
Figure S9: Pearson correlation coefficient (top), bias (middle; ppt), and centered RMSE (bottom; ppt) between posterior modelled and observed HFC-152a mole fractions above baseline at each measurement site for six inverse modelling systems (RHIME–NAME, RHIME–FLEXPART, ELRIS–NAME, ELRIS–FLEXPART, InTEM–NAME, InTEM–FLEXPART), using available site observations from 2013–2024 for NAME-based inversions and 2017–2024 for FLEXPART-based inversions.

HFC-245fa posterior model performance versus mole fraction observations above baseline
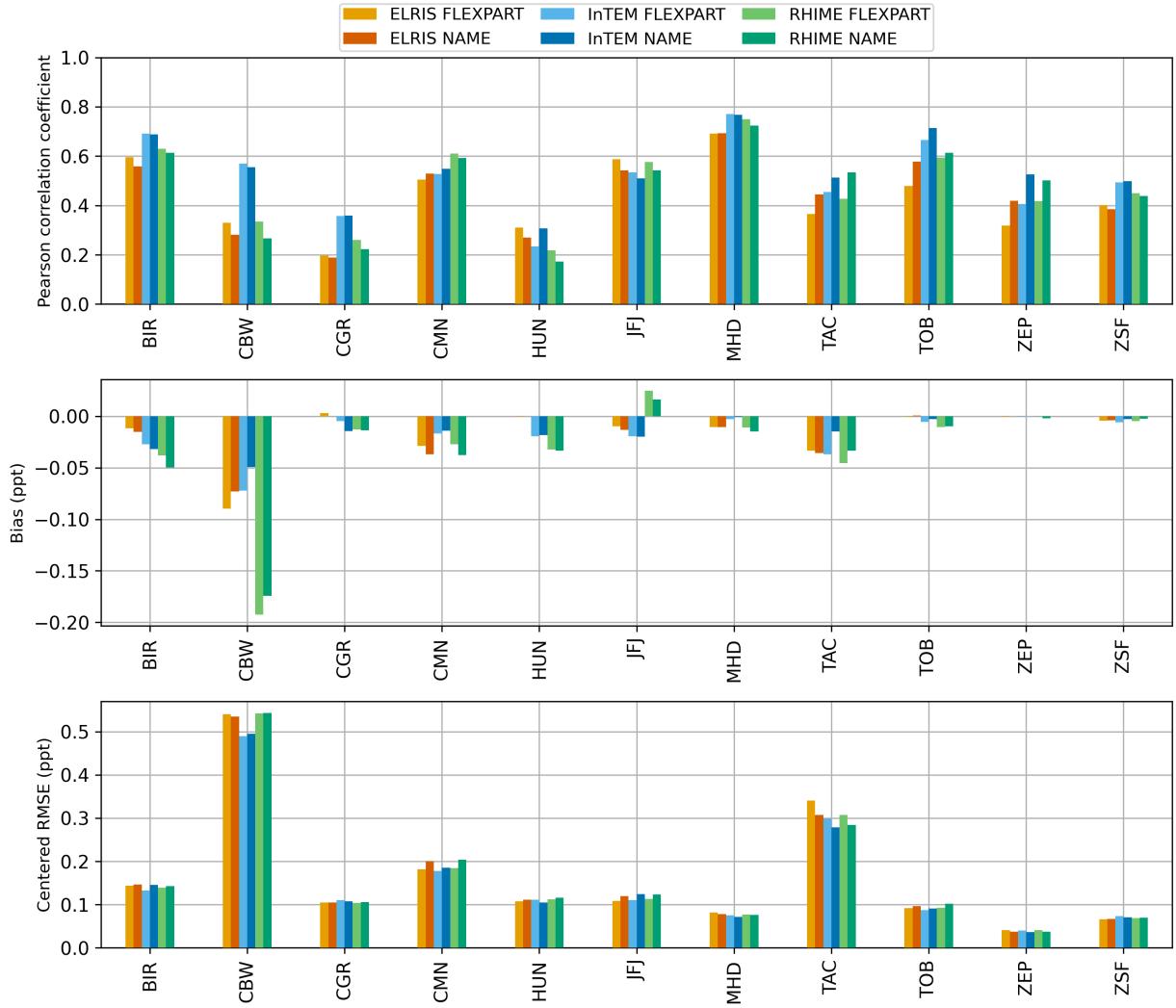
Figure S10: Pearson correlation coefficient (top), bias (middle; ppt), and centered RMSE (bottom; ppt) between posterior modelled and observed HFC-152a mole fractions above baseline at each measurement site for six inverse modelling systems (RHIME–NAME, RHIME–FLEXPART, ELRIS–NAME, ELRIS–FLEXPART, InTEM–NAME, InTEM–FLEXPART), using available site observations from 2013–2024 for NAME-based inversions and 2017–2024 for FLEXPART-based inversions.
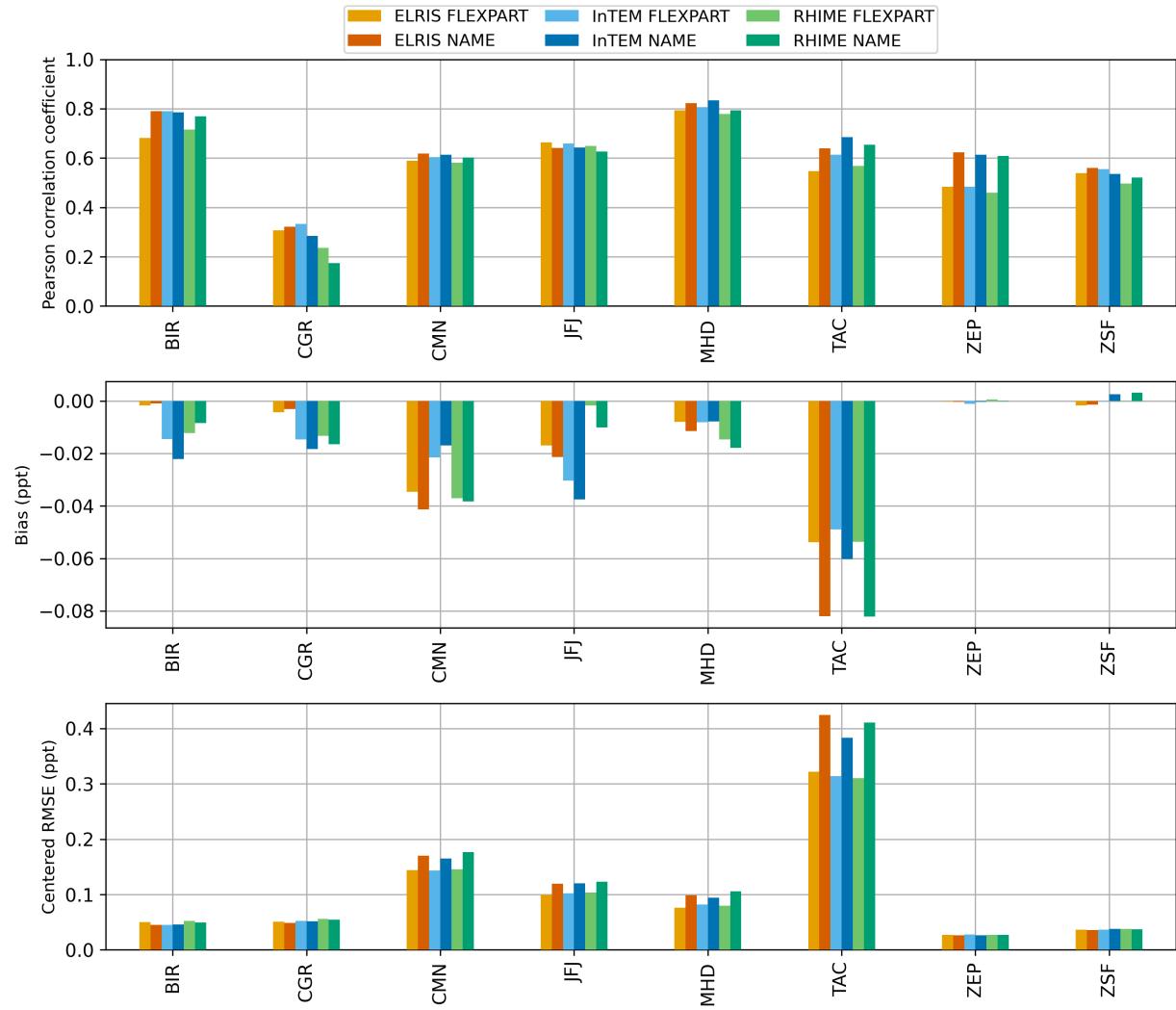
Figure S11: Pearson correlation coefficient (top), bias (middle; ppt), and centered RMSE (bottom; ppt) between posterior modelled and observed HFC-152a mole fractions above baseline at each measurement site for six inverse modelling systems (RHIME–NAME, RHIME–FLEXPART, ELRIS–NAME, ELRIS–FLEXPART, InTEM–NAME, InTEM–FLEXPART), using available site observations from 2013–2024 for NAME-based inversions and 2017–2024 for FLEXPART-based inversions.
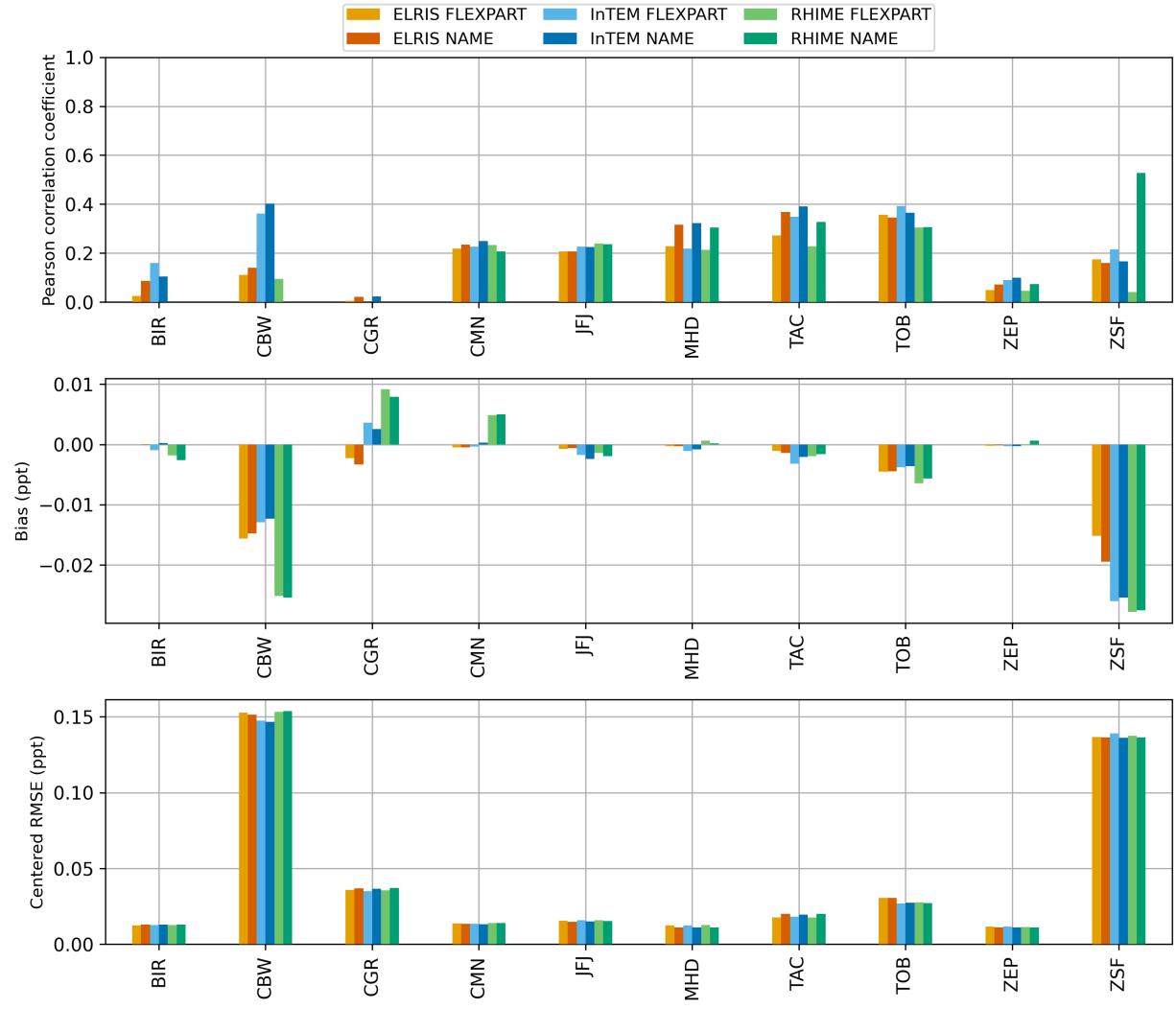
Figure S12: Pearson correlation coefficient (top), bias (middle; ppt), and centered RMSE (bottom; ppt) between posterior modelled and observed HFC-152a mole fractions above baseline at each measurement site for six inverse modelling systems (RHIME–NAME, RHIME–FLEXPART, ELRIS–NAME, ELRIS–FLEXPART, InTEM–NAME, InTEM–FLEXPART), using available site observations from 2013–2024 for NAME-based inversions and 2017–2024 for FLEXPART-based inversions.

References

[1] J. Hoker et al. "Comparison of GC/time-of-flight MS with GC/quadrupole MS for halocarbon trace gas analysis". In: *Atmospheric Measurement Techniques* 8.5 (2015), pp. 2195–2206. DOI: 10.5194/amt-8-2195-2015. URL: https://amt.copernicus.org/articles/8/2195/2015/.

[2] Andrew Jones et al. "The U.K. Met Office's Next-Generation Atmospheric Dispersion Model, NAME III". In: *Air Pollution Modeling and Its Application XVII*. Springer US, pp. 580–589. ISBN: 9780387282558. DOI: 10.1007/978-0-387-68854-1_62.

[3] M. Maione et al. "Ten years of continuous observations of stratospheric ozone depleting gases at Monte Cimone (Italy) — Comments on the effectiveness of the Montreal Protocol from a regional perspective". In: *Science of The Total Environment* 445-446 (2013), pp. 155–164. ISSN: 0048-9697. DOI: https://doi.org/10.1016/j.scitotenv.2012.12.056. URL: https://www.sciencedirect.com/science/article/pii/S0048969712016130.

[4] Alistair J. Manning et al. "Evidence of a recent decline in UK emissions of hydrofluorocarbons determined by the InTEM inverse model and atmospheric measurements". In: *Atmospheric Chemistry and Physics* 21.16 (Aug. 2021), pp. 12739–12755. ISSN: 1680-7324. DOI: 10.5194/acp-21-12739-2021.

[5] T. J. Schuck et al. "Establishing long-term measurements of halocarbons at Taunus Observatory". In: *Atmospheric Chemistry and Physics* 18.22 (2018), pp. 16553–16569. DOI: 10.5194/acp-18-16553-2018. URL: https://acp.copernicus.org/articles/18/16553/2018/.

[6] T. J. Schuck et al. "Greenhouse gas analysis of air samples collected onboard the CARIBIC passenger aircraft". In: *Atmospheric Measurement Techniques* 2.2 (2009), pp. 449–464. DOI: 10.5194/amt-2-449-2009. URL: https://amt.copernicus.org/articles/2/449/2009/.

[7] A. Stohl et al. "Technical note: The Lagrangian particle dispersion model FLEXPART version 6.2". In: *Atmospheric Chemistry and Physics* 5.9 (2005), pp. 2461–2474. DOI: 10.5194/acp-5-2461-2005.

[8] A. Tipka, L. Haimberger, and P. Seibert. "Flex_extract v7.1.2 – a software package to retrieve and prepare ECMWF data for use in FLEXPART". In: *Geosci. Model Dev.* 13.11 (2020), pp. 5277–5310. DOI: 10.5194/gmd-13-5277-2020. URL: https://gmd.copernicus.org/articles/13/5277/2020/https://gmd.copernicus.org/articles/13/5277/2020/gmd-13-5277-2020.pdf.